PHYSICAL REVIEW MATERIALS **6**, 044201 (2022)

Observation of a smoothly tunable Dirac point in Ge(Bi$_x$Sb$_{1\text{-}x}$)$_2$Te$_4$

Sean Howard,[1] Arjun Raghavan,[1] Davide Iaia,[1] Caizhi Xu,[1] David Flötotto,[1] Man-Hong Wong,[1] Sung-Kwan Mo,[2]
Bahadur Singh,[3] Raman Sankar,[4] Hsin Lin,[4] Tai-Chang Chiang,[1] and Vidya Madhavan[1,*]
[1]*Department of Physics and Frederick Seitz Materials Research Laboratory, University of Illinois at Urbana-Champaign, Urbana, Illinois, USA*
[2]*Advanced Light Source, Lawrence Berkeley National Laboratory, Berkeley, California, USA*
[3]*Department of Condensed Matter Physics and Materials Science, Tata Institute of Fundamental Research, Mumbai 400005, India*
[4]*Institute of Physics, Academia Sinica, Taipei, Taiwan 11529*

(Received 13 January 2021; revised 21 December 2021; accepted 11 January 2022; published 25 April 2022)

State-of-the-art topological devices require the use of topologically protected surface states to drive electronic transport. In this paper, we examine a tunable topological system, Ge(Bi$_x$Sb$_{1\text{-}x}$)$_2$Te$_4$, for a range of x values from 0 to 1, using a combination of Fourier transform scanning tunneling spectroscopy and angle-resolved photoemission spectroscopy. Our results show that the Dirac point shifts linearly with x, crossing the Fermi energy near $x = 0.7$. This observation of a smoothly tunable, isolated Dirac point crossing through the topological transport regime and having strong linear dependence with substitution can be critical for future topological spintronics applications.

DOI: 10.1103/PhysRevMaterials.6.044201

I. INTRODUCTION

Since the discovery of topological materials, much effort has been made to utilize the properties of topologically protected states in electronic devices [1–7]. Among the primary challenges in realizing such devices is the isolation of topological surface states (TSSs) from a background of trivial bulk states [1–3]. If the chemical potential intersects bulk valence or conduction bands, transport will be dominated by bulk contributions [8]. To avoid this, the chemical potential must be manipulated into the bandgap containing topological states, while keeping the band topology nontrivial.

One method to achieve transport dominated by topological states is chemical substitution. This type of topological engineering has been previously studied in material systems including Bi$_{2\text{-}x}$Sb$_x$Te$_{3\text{-}y}$Se$_y$, (Bi$_{1\text{-}x}$Sb$_x$)$_2$Te$_3$, and BiTl(S$_{1\text{-}x}$Se$_x$)$_2$ [9–11]. In these materials, substitution moves the system into the topological transport regime, where transport is dominated by spin-polarized topological states [9,11]. However, the systems previously studied have several challenges [12] associated with them, including difficulty in growth of materials and abrupt changes in Dirac point energy values. This motivates the study of new materials for topological engineering, and in this paper, we study one such system Ge(Bi$_x$Sb$_{1\text{-}x}$)$_2$Te$_4$.

Several properties of Ge(Bi$_x$Sb$_{1\text{-}x}$)$_2$Te$_4$ suggest the potential for tuning its topological states by substitution, making it ideal for optimizing the band structure to achieve transport dominated by the topological bands. Of the two parent compounds, GeBi$_2$Te$_4$ and GeSb$_2$Te$_4$, of this system, GeBi$_2$Te$_4$ is known to be a topological insulator with a bandgap of ≈200 meV and an isolated Dirac point 280 meV below the Fermi energy [13]. This is advantageous since an isolated Dirac point is a critical component of electrical transport dominated by TSSs. On the other end, time- and spin-resolved angle-resolved photoemission spectroscopy (ARPES) have also recently shown GeSb$_2$Te$_4$ to be topologically nontrivial, with a Dirac point ∼450 meV above the Fermi energy [14].

Other material properties also contribute to technological interest in the system. Both parent compounds of this system are known thermoelectric materials [15]. In addition, GeSb$_2$Te$_4$ is a phase-change material which enters a metastable rock-salt phase by rapid cooling, suggesting possible use in nonvolatile random-access memory devices [16,17]. Finally, a large spin polarization is measured in the TSS of GeBi$_2$Te$_4$ by spin-resolved ARPES [18], which can be important for increased efficiency of spintronics devices. Detailed experimental studies of the effects of substitution in Ge(Bi$_x$Sb$_{1\text{-}x}$)$_2$Te$_4$ are therefore critically needed to understand its potential utility in a variety of electronic and spintronic applications.

II. EXPERIMENTAL METHODS

In this paper, a combination of Fourier transform scanning tunneling spectroscopy (FT-STS) and ARPES is used to investigate Ge(Bi$_x$Sb$_{1\text{-}x}$)$_2$Te$_4$. ARPES measurements were carried out at the BL 10.0.1 at the Advanced Light Source in Lawrence Berkeley National Laboratory. To investigate the band structure of unoccupied states above the Fermi energy and to confirm ARPES results below the Fermi energy, FT-STS is used. FT-STS measurements are performed at 4 K with a scanning tunneling microscope (STM) in ultrahigh vacuum; bulk single crystals are cleaved *in situ* and measured with annealed W STM tips. Since STM dI/dV spectra can

---

[*] vm1@illinois.edu

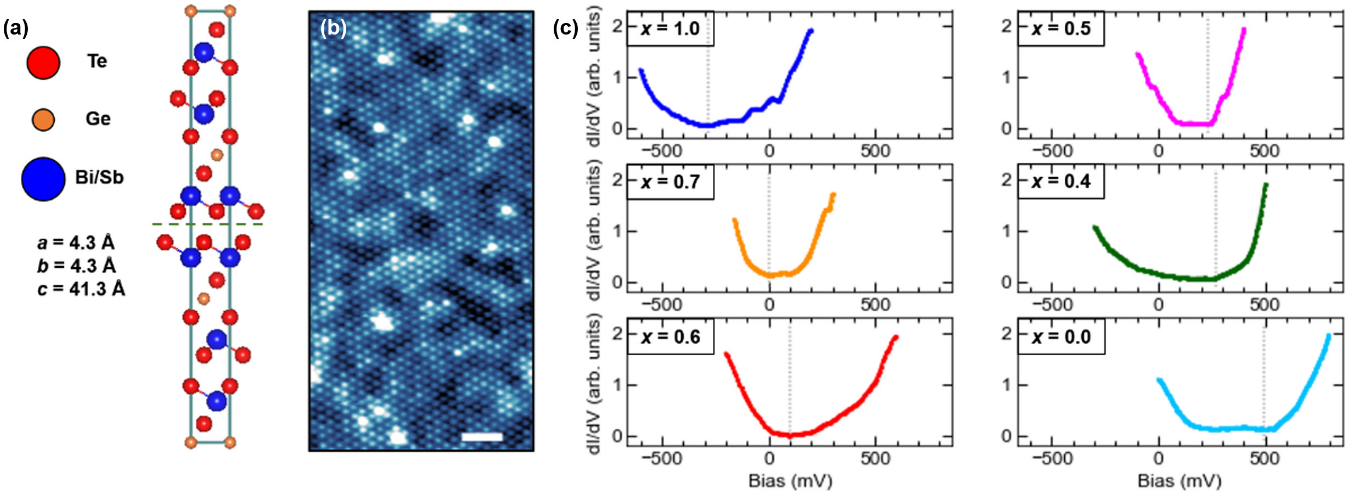

FIG. 1. Crystal structure, scanning tunneling microscopy (STM) topography, and dI/dV spectra. (a) Crystal structure of Ge$(\mathrm{Bi}_x\mathrm{Sb}_{1\text{-}x})_2Te_4$; dashed line shows cleaving plane between two van der Waals bonded Te layers. (b) 10 × 20 nm topography ($I_T = 110$ pA, $V_{\mathrm{Bias}} = -400$ mV) of Ge$(\mathrm{Bi}_{0.4}\mathrm{Sb}_{0.6})_2Te_4$ showing a hexagonal lattice structure from the exposed Te surface. (c) STM dI/dV spectra for Bi substitutions of $x = 0.0$, 0.4, 0.5, 0.6, 0.7, and 1.0; the differences between the spectra reflect changes in the band structure due to doping. The minimum of the spectra shifts monotonically to higher energies with decreasing x, crossing the Fermi energy ($V_{\mathrm{Bias}} = 0$ mV) near $x = 0.7$. The minima are marked by the light gray dotted lines.

be highly dependent on tip conditions, we use the same, unmodified tungsten STM tip for taking spectra across the substitutions measured in this work, except for the end members of the Ge$(\mathrm{Bi}_x\mathrm{Sb}_{1-x})_2Te_4$ series, which were part of a separate measurement run. Details of crystal growth are given in the Appendix. Supplementary electrical transport measurements were performed using a 4-point contact method with a Quantum Design DynaCool Physical Property Measurement System.

The FT-STS technique utilizes quasiparticle interference (QPI) in the material, occurring due to quasiparticle scattering from defects and other imperfections and yielding energy-dependent standing waves [19]. While direct backscattering is in general prohibited for TSSs, due to the effects of hexagonal warping, a significant QPI signal is generated in Ge$(\mathrm{Bi}_x\mathrm{Sb}_{1\text{-}x})_2Te_4$ [12,20,21]. Similar warping effects have been previously observed in Bi$_2$Te$_3$ [21] and GeBi$_2$Te$_4$ [22], for example. Using the measured QPI scattering vectors, momentum-space band structure information is obtained. The combination of FT-STS and ARPES thus provides a powerful means to understand changes in the topological properties of the Ge$(\mathrm{Bi}_x\mathrm{Sb}_{1\text{-}x})_2Te_4$ system.

III. RESULTS AND DISCUSSION

Ge$(\mathrm{Bi}_x\mathrm{Sb}_{1\text{-}x})_2Te_4$ crystals consist of stacked hexagonal layers forming a unit cell with $c = 41.3$ Å [22], as shown in Fig. 1(a). To characterize the surface, we obtain STM images of the cleaved crystals. The sample cleaves between van der Waals bonded Te layers, as indicated in Fig. 1(a). A typical STM topography scan obtained on one of the materials in our series GeBi$_{0.8}$Sb$_{1.2}$Te$_4$ shows the hexagonal lattice expected for these surfaces [Fig. 1(b)]; topography scans for all other substitutions are shown in the Appendix. Figure 1(c) shows STS dI/dV spectra, representing the local density of states (LDOS), for substitutions ranging from $x = 0.0$ to 1.0. The spectra are found to have major differences in locations of their minima. These reflect significant changes in the band structure due to substitution and motivate further investigation using ARPES and FT-STS. More specifically, the Dirac point can be given [23] by the minimum of a dI/dV spectrum, which corresponds to the LDOS. In this paper, we show very strong agreement between Dirac point values found from our ARPES measurements, previously published ARPES spectra, and our STM dI/dV measurements. At $x = 1.0$, the STM dI/dV minimum occurs at −280 meV, in agreement with the −280 meV ARPES measurement by Arita *et al.* [22]. For $x = 0.7$, the lowest point of the LDOS is very close to the Fermi energy ($V_{\mathrm{Bias}} = 0$ mV), with a dI/dV minimum value of 4 meV. Further Sb substitution continues to monotonically shift the minimum to larger, positive energies, with GeSb$_2$Te$_4$ showing a dI/dV minimum at 492 meV. This agrees with the recent time- and spin-resolved ARPES results of Nurmamat *et al.* [14], showing the Dirac point to be ~450 meV above the Fermi energy.

While the STM dI/dV results suggest that the $x = 0.7$ substitution could place Ge$(\mathrm{Bi}_x\mathrm{Sb}_{1\text{-}x})_2Te_4$ in the topological transport regime, a dI/dV minimum may not, in itself, be sufficient evidence. Hence, we next measure the band structure of Ge$(\mathrm{Bi}_x\mathrm{Sb}_{1\text{-}x})_2Te_4$ for the compositions $x = 1$, 0.7, 0.6, 0.5, and 0.4 using ARPES. Figure 2(a) shows ARPES data for $x = 1$, that is, GeBi$_2$Te$_4$, along the Γ-K direction. The intensity below a binding energy of 0.6 eV is from the bulk valence band. We also observe the contribution from the conduction band near the chemical potential. Surface states with approximate linear dispersion are seen to cross at a Dirac point near the center of the Brillouin zone. The ARPES spectra for substitutions Ge$(\mathrm{Bi}_x\mathrm{Sb}_{1\text{-}x})_2Te_4$ from $x = 0.7$ down to 0.4 are shown in Figs. 2(b)–2(e). At all compositions, we observe the presence of quasilinearly dispersing in-gap states, with $x =$ 1.0 and 0.7 data allowing for linear fitting; this fitting is shown in Fig. 8. We note that the slopes of the lines, which yield the

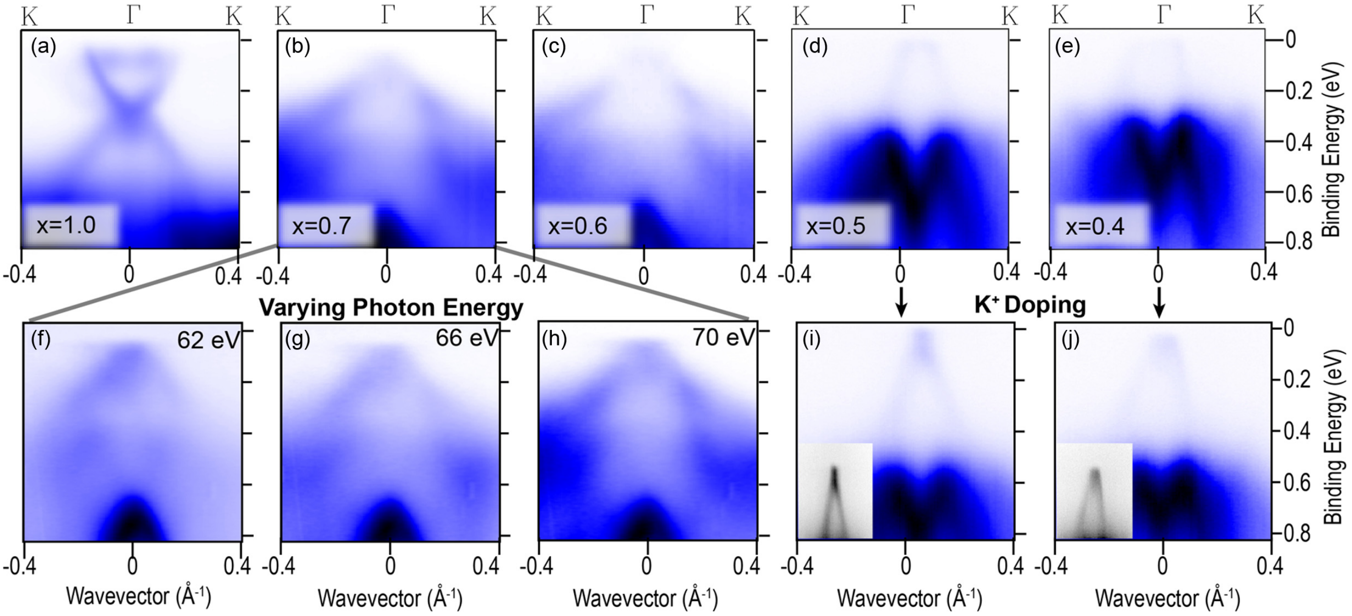

FIG. 2. Angle-resolved photoemission spectroscopy (ARPES) measurements. (a)–(e) ARPES data along the Γ-K direction with different values of Bi doping x for Ge(Bi$_x$Sb$_{1-x}$)$_2$Te$_4$. (f)–(h) GeBi$_{1.4}$Sb$_{0.6}$Te$_4$ ARPES spectra with varying values of the incoming photon energy; the lack of change in the band structure suggests that the measured intensity is from two-dimensional topological surface states. (i)–(j) ARPES measurements of potassium surface-doped samples with $x = 0.5$ and 0.4; K deposition shifts the Fermi energy, making the Dirac point visible. Insets are close-ups of the spectra near the Dirac point.

Fermi velocities, change with substitution. Moreover, we confirm that the in-gap states seen are two-dimensional surface states by varying the incoming photon energy between 62 and 70 eV. As demonstrated for GeBi$_{1.4}$Sb$_{0.6}$Te$_4$ in Figs. 2(f)–2(h), with changing phonon energy, the in-gap states do not change significantly, while there are clear changes in the bulk valence bands at higher binding energies. To obtain further insights into the evolution of the band structure with Sb substitution, we shift the position of E_F relative to the Dirac cone by depositing potassium on the surface [Figs. 2(i)–2(j)]. This allows us to see the lower part of the Dirac cone clearly, although further confirmation of the band structure above the Fermi energy is still necessary.

For identifying states in the upper part of the Dirac cone, and for comparison with ARPES data, FT-STS QPI scattering is employed. Slices of LDOS maps in GeBi$_{1.4}$Sb$_{0.6}$Te$_4$ at 200 and 100 meV of size 60 × 60 nm are shown in Figs. 3(a) and 3(b). We perform FTs of each of these maps for analysis. In Ge(Bi$_x$Sb$_{1-x}$)$_2$Te$_4$, scattering between the hexagonally warped surface bands yields a significant QPI signal [20]. The states found through FT-STS are identifiable as TSSs from their close resemblance to related materials such as Bi$_2$Te$_3$, along with their symmetry [21,23]. Due to the spin texture, the signal is dominated by scattering across vectors connecting alternating Γ-K bands, resulting in scattering vectors along the Bragg peak Γ-M direction [20]; this scattering geometry is shown in Fig. 3(e). In Figs. 3(c) and 3(d), the FTs of the LDOS maps at 200 and 100 meV are presented. The Bragg peaks are visible at the corners of the FTs, and the scattering wave vectors occur only in these Γ-M directions. Moreover, a significant change in the wave vectors is seen as a function of energy: as the energy is increased, the wave vectors get larger, indicating a positive dispersion. In the smaller energy 100 to −100 meV range, FTs of dI/dV slices do not show clear scattering vectors.

We now compare data from the STM dI/dV and ARPES measurements. The Dirac point energy is shown to have a

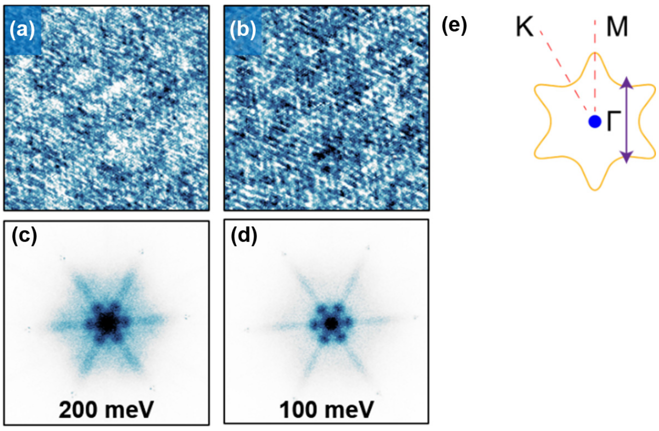

FIG. 3. dI/dV maps, Fourier transforms (FTs), and scattering schematic. (a) and (b) 60 nm^2 energy slices of a dI/dV map at 200 and 100 meV, respectively, for GeBi$_{1.4}$Sb$_{0.6}$Te$_4$. (c) and (d) FTs of dI/dV map slices in (a) and (b). The six Bragg peaks appear as dots near the outside of the slices, while the surface state quasiparticle interference (QPI) scattering vectors appear as brighter spots closer to the center. It is evident that the scattering vectors disperse with energy, while the Bragg peaks stay constant; the scattering vectors are identified as arising from the surface states due to their dispersion and close resemblance to the hexagonally symmetric surface state QPI vectors in related materials such as Bi$_2$Te$_3$. (e) Schematic of hexagonally warped surface band structure; magenta arrow shows possible scattering vector along the Bragg peak Γ-M direction.

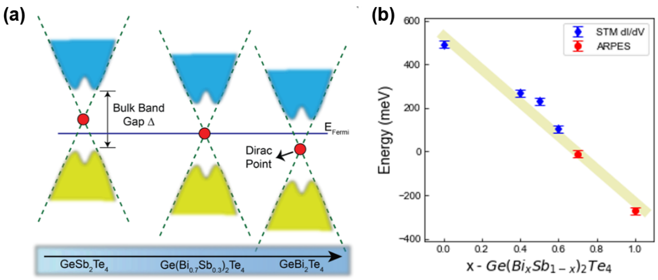

FIG. 4. Band structure evolution and shift of the Dirac point. (a) Schematic of band structure evolution as Sb is substituted with Bi. The linearly dispersing topological surface states intersect at the Dirac point, which shifts and crosses the Fermi energy near the $GeBi_{1.4}Sb_{0.6}Te_4$ substitution. (b) Plot of Dirac point energies, as determined by angle-resolved photoemission spectroscopy (ARPES; red circles) and using the minima of scanning tunneling microscopy (STM) dI/dV spectra (blue diamonds). The energies are shown to have a strong linear dependence on the substitution x in $Ge(Bi_xSb_{1-x})_2Te_4$, with linear fitting yielding an R^2 value of 0.98.

strong linear dependence with doping; the Dirac point values and fitting are shown in Fig. 4(b). An R^2 value of 0.98 is obtained for the linear fit. As shown in the schematic of Fig. 4(a) and proven using a combination of FT-STS and ARPES, the topologically nontrivial band structure remains throughout the range of substitutions. The Dirac point crosses the Fermi energy very close to the $x = 0.7$ doping. This combination of an isolated Dirac point along with its location within only 10 meV of the Fermi energy makes $GeBi_{1.4}Sb_{0.6}Te_4$ an ideal alloy for topological transport and spintronic [5] applications.

IV. CONCLUSIONS

In conclusion, in this detailed paper, employing a combination of STM, ARPES, and FT-STS, we have experimentally revealed a tunable topological insulator system $Ge(Bi_xSb_{1-x})_2Te_4$, a valuable addition to existing work on other pseudobinary systems [24–28]. The ability to smoothly tune the Dirac point as a linear function of substitution, without abrupt changes found in other related systems [13], will allow for topological transport applications [29] for this series of materials. Future work, especially on the $GeBi_{1.4}Sb_{0.8}Te_4$ alloy, which resides at an ideal position in the topological transport regime, can examine technologically significant properties such as topological transmission through surface barriers, like previous measurements, for example, on Sb(111) [30]. The topology of $Ge(Bi_xSb_{1-x})_2Te_4$ thus provides a unique platform for a number of novel fundamental studies and technological applications.

TABLE I. Crystal stoichiometries. Compositions of $Ge(Bi_xSb_{1-x})_2Te_4$ samples are tested using an electron probe micro-analyzer technique. All measured compositions are very close to the nominal value with an average difference of only 4.4%.

x (nominal)	x (actual)
1.00	1.00
0.70	0.68
0.60	0.56
0.50	0.51
0.40	0.38
0.00	0.04

ACKNOWLEDGMENTS

The STM measurements were supported by the National Science Foundation (NSF) under Grant No. 1711875. V.M. acknowledges partial support from the Gordon and Betty Moore Foundation's EPiQS Initiative through Grant No. GBMF9465. The work in this paper was carried out, in part, at the Seitz Materials Research Laboratory Central Research Facilities, at the University of Illinois at Urbana-Champaign. The ARPES work is supported by the DOE, OS, BES, Division of Materials Science and Engineering, under Grant No. DE-FG02-07ER46383 (T.-C.C.). This ARPES work used resources of the Advanced Light Source, which is a DOE, OS, User Facility under Contract No. DE-AC02-05CH11231. H.L. and R.S. acknowledge support from the Taiwan Ministry of Science and Technology (MOST) under Grants No. 109-2112-M-001-014-MY3 and No. MOST-108-2112-M-001-049-MY2, respectively.

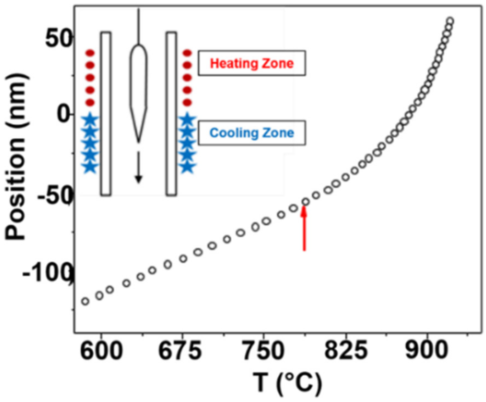

FIG. 5. Single crystal growth. Temperature profile of the cooling process vs the relative position of sample. Inset shows a schematic of our vertical Bridgman furnace.

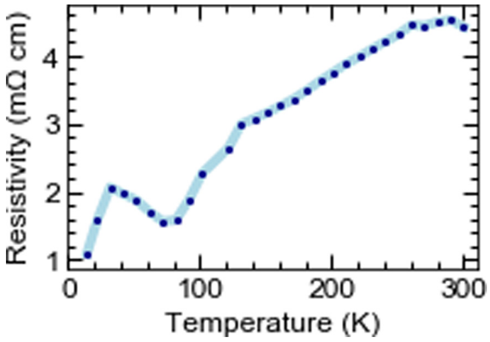

FIG. 6. Electrical transport characterization of $GeBi_2Te_4$. Electrical resistivity characterization of $GeBi_2Te_4$ shows relatively high mobility and an increase in resistivity as the temperature is decreased <90 K, in close agreement with previous results from Marcinkova *et al.* (2013) [24].

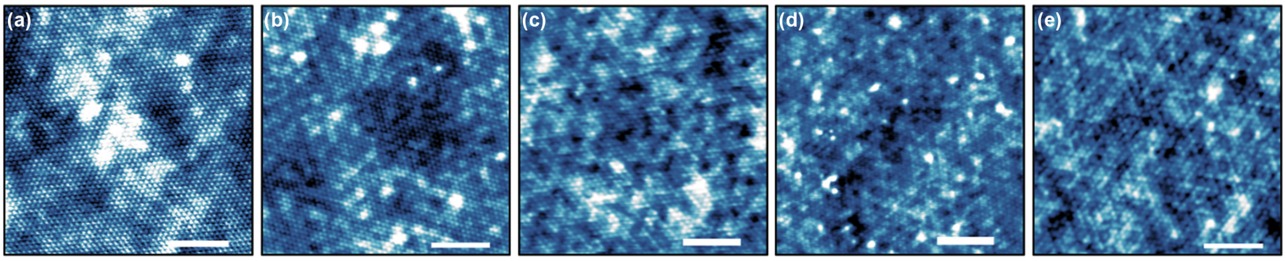

FIG. 7. 20 × 20 nm topography scans at different substitutions. (a) Topography of $GeSb_2Te_4$ with 80 pA and -100 mV. (b) Topography of $GeBiSbTe_4$ with 60 pA and -100 mV. (c) Topography of $GeBi_{1.2}Sb_{0.8}Te_4$ with 100 pA and 300 mV. (d) Topography of $GeBi_{1.4}Sb_{0.6}Te_4$ with 60 pA and -210 mV. (e) Topography of $GeBi_2Te_4$ with 360 pA and -250 mV.

APPENDIX

1. Crystal growth

The highly oriented single crystals of Ge(Bi$_x$Sb$_{1\text{-}x}$)$_2$Te$_4$ are grown by using the vertical Bridgman method. Initially, stoichiometric mixtures of Ge(Bi$_x$Sb$_{1\text{-}x}$)$_2$Te$_4$ compounds were prepared with high-purity metal precursors (5N) of bismuth (Bi), antimony (Sb), germanium (Ge), and tellurium (Te). These initial powders of Ge(Bi$_x$Sb$_{1\text{-}x}$)$_2$Te$_4$ were calcinated at 800 °C for 24 h in a crucible furnace and then cooled down to room temperature slowly. Further finely ground compounds were transferred in carbon coated quartz tubes for highly oriented single-crystal growth under an Ar atmosphere purged environment and sealed under a vacuum of $\approx 2 \times 10^{-3}$ Torr. These double-sealed quartz tube powders were then heated at 900 °C for 200 h in a vertical Bridgman furnace to grow single crystals. The schematic of the crystal growth setup is shown in the inset of Fig. 5. A temperature gradient of ≈0.5 °C/mm is programmed at near the solidification point (marked by the red arrow in Fig. 5), and the quartz tubes are then moved slowly into the cooling zone with a translation rate close to 0.2 mm/h. We have monitored and measured the temperature profile of the cooling process vs the relative position of the sample using an R-type thermocouple, as displayed in Fig. 5.

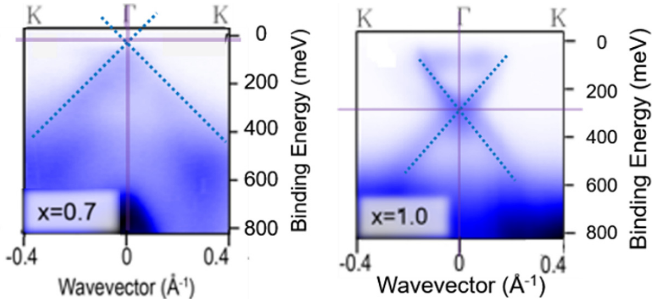

FIG. 8. ARPES fitting. Linear fitting of ARPES spectra, by using MATLAB for processing, yields high R^2 values > 0.90, and Dirac points of -6 meV for $x = 0.7$, and -272 meV for $x = 1.0$. For better fitting clarity, we use the 66 eV photon energy spectrum for the $x = 0.7$ case. Fitting is only used for the two substitutions shown above since the Dirac cone is not clear for other values. Hence, for $x = 0.6$, 0.5, 0.4, and 0.0, the Dirac point energies are extracted from scanning tunneling microscopy (STM) dI/dV spectra.

2. Sample stoichiometry

Samples of different compositions are grown in this paper. However, the nominal stoichiometry may differ from the actual stoichiometry [31]. To test that our actual compositions are close to the nominal values, we use an electron probe micro-analyzer technique.

As shown in Table I, all crystal compositions are very close to the corresponding nominal values, yielding an average

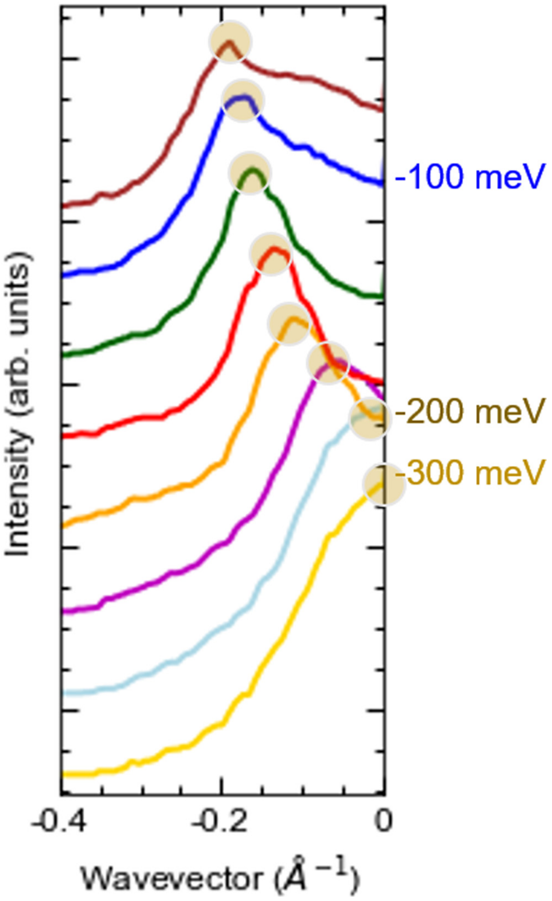

FIG. 9. ARPES momentum distribution curves. Momentum distribution curves (MDCs) from ARPES measurements of $GeBi_2Te_4$ ($x = 1.0$); maxima are marked by circles. Linear fitting is shown in Fig. 8, and as shown above, the MDCs have a clear linear dispersion from the Fermi energy down to ~ -200 meV. Although the material is a topological insulator, a deviation from linear dispersion can be seen < -200 meV and may occur due to hexagonal warping.

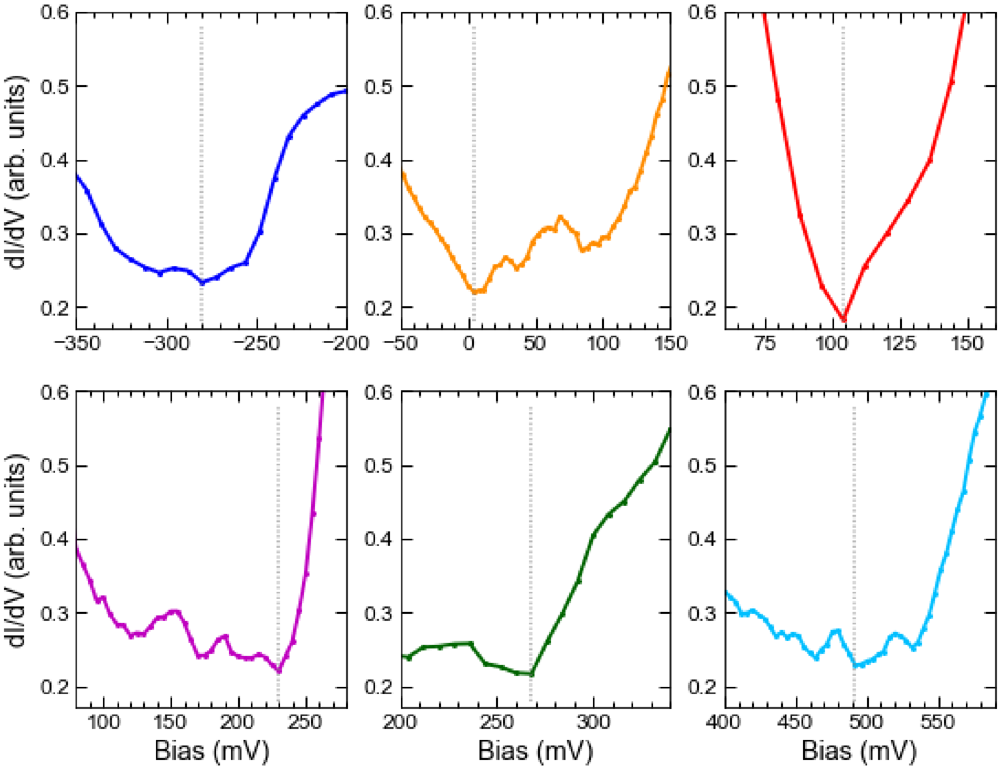

FIG. 10. Scanning tunneling microscopy (STM) dI/dV spectra minima. Zoomed-in STM dI/dV spectra close to the minima, for the six spectra presented in Fig. 1(c); gray dotted lines show the minimum energy values. While ARPES spectra are used to extract the Dirac point energy for $x = 1.0$ and 0.7, the minima from the STM dI/dV spectra are used for $x = 0.6$, 0.5, 0.4, and 0.0, yielding Dirac point energy values of 104, 230, 268, and 492 meV, respectively. In addition, we find a minimum value of 4 meV for $x = 0.7$, in close agreement with the Dirac point energy of −6 meV extracted from linear fitting of ARPES spectra.

difference of only 4.4%. Hence, we confirm that our actual crystal compositions match well with nominal x values of 1.00, 0.70, 0.60, 0.50, 0.40, and 0.00.

3. $GeBi_2Te_4$ electrical transport measurements

Electrical transport measurements are performed on $GeBi_2Te_4$ to further characterize the material, especially in the context of potential use in future technological applications. We find, as shown in Fig. 6, a relatively high mobility throughout the temperature range, with resistivity <5 mΩ cm, even at 300 K. The resistivity follows a monotonic decrease from 300 down to 90 K, followed by an increase, and further decrease $< \sim 50$ K, consistent with previous resistivity data reported by Marcinkova *et al.* [24].

4. $Ge(Bi_xSb_{1-x})_2Te_4$ STM topography scans

STM topography scans at all substitutions are presented in this paper; while $x = 0.4$ is shown in the main text, 20 × 20 nm scans for $x = 0.0$, 0.5, 0.6, 0.7, and 1.0 are given in Fig. 7. As is evident, there is a significant degree of electronic disorder across all substitutions. However, we can find large, flat atomically resolved areas for measurements at all substitutions.

5. ARPES spectra fitting and momentum distribution curves

Linear fitting of ARPES spectra is shown in Fig. 8. We use MATLAB image processing and fitting capabilities to find high R^2 values >0.9. Our linear fits yield Dirac point energy values of −272 meV for $x = 1.0$ and −6 meV for $x = 0.7$. The −272 meV value agrees well with previously reported ARPES results [22] on $GeBi_2Te_4$. A corresponding set of momentum distribution curves is shown in Fig. 9, for $x = 1.0$.

6. STM dI/dV spectra minima and dI/dV spectra relative to Dirac points

We show, in Fig. 10, zoomed-in STM dI/dV spectra near the minima for each of the six substitutions measured. The full spectra are shown in Fig. 1(c). Our minima, which represent the energy values of the Dirac points, are 104, 230, 268, and 492 meV, for $x = 0.6$, 0.5, 0.4, and 0.0, respectively. The $x = 0.0$ value agrees with the ARPES-derived Dirac point value of ≈450 meV found by Nurmamat *et al.* [14]. Moreover, for $x = 0.7$, the STM dI/dV minimum is 4 meV, very close to the Fermi energy and in agreement with our ARPES value of −6 meV. For $x = 1.0$, the minimum is at −280 meV, again in very close agreement with our ARPES-measured value and that of Arita *et al.* [22]. In Fig. 11, we show dI/dV spectra plotted relative to the Dirac point of each substitution. A pattern can be found in the plot, with the valence band shifting closer to the Dirac point energy and the conduction band shifting farther from the Dirac point energy as x increases. Hence, while the bulk properties of the material change significantly with substitution, the Dirac cone in this material system can be tuned continuously and smoothly.

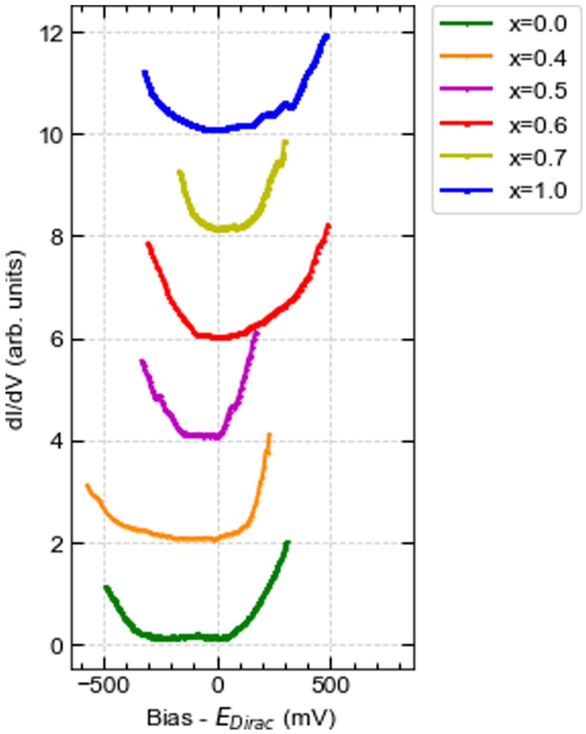

FIG. 11. Scanning tunneling microscopy (STM) dI/dV spectra relative to Dirac points. STM spectra from $x = 0.0$ on the bottom to $x = 1.0$ on the top, with offsets of 2, plotted relative to the Dirac point energy at each substitution. A pattern is visible, with the conduction bands shifting farther from the Dirac point, and the valence bands shifting closer to the Dirac point, as x is increased.

---

[1] D. Qu, Y. S. Hor, J. Xiong, R. J. Cava, and N. P. Ong, Quantum oscillations and Hall anomaly of surface states in the topological insulator Bi_2Te_3, Science **329**, 821 (2010).

[2] Y. S. Hor, J. G. Checkelsky, D. Qu, N. P. Ong, and R. J. Cava, Superconductivity and non-metallicity induced by doping the topological insulators Bi_2Se_3 and Bi_2Te_3, J. Phys. Chem. Solids **72**, 572 (2011).

[3] P. Ghaemi, R. S. K. Mong, and J. E. Moore, In-Plane Transport and Enhanced Thermoelectric Performance in Thin Films of the Topological Insulators Bi_2Te_3 and Bi_2Se_3, Phys. Rev. Lett. **105**, 166603 (2010).

[4] B. Singh, H. Lin, R. Prasad, and A. Bansil, Topological phase transition and two-dimensional topological insulators in Ge-based thin films, Phys. Rev. B **88**, 195147 (2013).

[5] D. Pesin and A. H. MacDonald, Spintronics and pseudospintronics in graphene and topological insulators, Nat. Mater. **11**, 409 (2012).

[6] J. Han, A. Richardella, S. Siddiqui, J. Finley, N. Samarth, and L. Liu, Room-Temperature Spin-Orbit Torque Switching Induced by a Topological Insulator, Phys. Rev. Lett. **119**, 077702 (2017).

[7] A. Kandala, A. Richardella, D. W. Rench, D. M. Zhang, T. C. Flanagan, and N. Samarth, Growth and characterization of hybrid insulating ferromagnet-topological insulator heterostructure devices, Appl. Phys. Lett. **103**, 202409 (2013).

[8] J. G. Checkelsky, Y. S. Hor, R. J. Cava, and N. P. Ong, Bulk Band Gap and Surface State Conduction Observed in Voltage Tuned Crystals of the Topological Insulator Bi_2Se_3, Phys. Rev. Lett. **106**, 196801 (2011).

[9] T. Arakane, T. Sato, S. Souma, K. Kosaka, K. Nakayam, M. Komatsu, T. Takahashi, Z. Ren, K. Segawa, and Y. Ando, Tunable Dirac cone in the topological insulator $Bi_{2\text{-}x}Sb_xTe_{3\text{-}y}Se_y$, Nat. Commun. **3**, 636 (2012).

[10] D. Kong, Y. Chen, J. J. Cha, Q. Zhang, J. G. Analytis, K. Lai, Z. Liu, S. S. Hong, K. J. Koski, S. Mo *et al.*, Ambipolar field effect in the ternary topological insulator $(Bi_xSb_{1-x})_2Te_3$ by composition tuning, Nat. Nanotechnol. **6**, 705 (2011).

[11] S. Xu, Y. Xia, L. A. Wray, S. Jia, F. Meier, J. H. Dil, J. Osterwalder, B. Slomski, A. Bansil, H. Lin *et al.*, Topological phase transition and texture inversion in a tunable topological insulator, Science **332**, 560 (2011).

[12] Y. Ando, Topological insulator materials, J. Phys. Soc. Jpn. **82**, 102001 (2013).

[13] M. Neupane, S. Xu, L. A. Wray, A. Petersen, R. Shankar, N. Alidoust, C. Liu, A. Fedorov, H. Ji, J. M. Allred *et al.*, Topological surface states and Dirac point tuning in ternary topological insulators, Phys. Rev. B **85**, 235406 (2012).

[14] M. Nurmamat, K. Okamoto, S. Zhu, T. V. Menshchikova, I. P. Rusinov, V. O. Korostelev, K. Miyamoto, T. Okuda, T. Miyashita, X. Wang *et al.*, Topologically nontrivial phase-change compound $GeSb_2Te_4$, ACS Nano **14**, 9059 (2020).

[15] T. Schröeder, M. N. Schneider, T. Rosenthal, P. Urban, and F. Fahrnbauer, Thermoelectric properties of metastable Ge/Sb/Te and Ge/Bi/Te compounds, AIP Conf. Proc. **1449**, 159 (2012).

[16] T. Siegrist, P. Jost, H. Volker, M. Woda, P. Merkelbach, C. Schlockermann, and M. Wuttig, Disorder-induced localization in crystalline phase-change materials, Nat. Mater. **10**, 202 (2011).

[17] T. Matsunaga and N. Yamada, Structural investigation of $GeSb_2Te_4$: a high-speed phase-change material, Phys. Rev. B **69**, 104111 (2004).

[18] K. Okamoto, K. Kuroda, H. Miyahara, K. Miyamoto, T. Okuda, Z. S. Aliev, M. B. Babanly, I. R. Amiraslanov, K. Shimada, H. Namatame *et al.*, Observation of a highly spin-polarized topological surface state in $GeBi_2Te_4$, Phys. Rev. B **86**, 195304 (2012).

[19] J. E. Hoffman, Spectroscopic scanning tunneling microscopy insights into Fe-based superconductors, Rep. Prog. Phys. **74**, 124513 (2011).

[20] Z. Wang, Y. Chong, J. D. Joannopoulos, and M. Soljačić, Observation of unidirectional backscattering-immune topological electromagnetic states, Nature (London) **461**, 772 (2009).

[21] T. Zhang, P. Cheng, X. Chen, J. Jia, X. Ma, K. He, L. Wang, H. Zhang, X. Dai, Z. Fang *et al.*, Experimental Demonstration of Topological Surface States Protected by Time-Reversal Symmetry, Phys. Rev. Lett. **103**, 266803 (2009).

[22] M. Arita, H. Sato, K. Shimada, H. Namatame, M. Taniguchi, M. Sasaki, M. Kitaura, A. Ohnishi, and H. Kim, Angle resolved photoemission study of $GeBi_2Te_4$, JPS Conf. Proc. **1**, 012017 (2014).

[23] H. Beidenkopf, P. Roushan, J. Seo, L. Gorman, I. Drozdov, Y. S. Hor, R. J. Cava, and A. Yazdani, Spatial fluctuations of helical Dirac fermions on the surface of topological insulators, Nat. Phys. **7**, 939 (2011).

[24] A. Marcinkova, J. K. Wang, C. Slavonic, A. H. Nevidomskyy, K. F. Kelly, Y. Filinchuk, and E. Morosan, Topological metal behavior in $GeBi_2Te_4$ single crystals, Phys. Rev. B **88**, 165128 (2013).

[25] T. Matsunaga, N. Yamada, and Y. Kubota, Structures of stable and metastable Ge_2Sb_2Te, an intermetallic compound in GeTe-Sb_2Te_3 pseudobinary systems, Acta Cryst. B **60**, 685 (2004).

[26] J. Kellner, G. Bihlmayer, M. Liebmann, S. Otto, C. Pauly, J. E. Boschker, V. Bragaglia, S. Cecchi, R. N. Wang, V. L. Deringer *et al.*, Mapping the band structure of GeSbTe phase change alloys around the Fermi level, Commun. Phys. **1**, 5 (2018).

[27] C. Pauly, M. Liebmann, A. Giussani, J. Kellner, S. Just, J. Sanchez-Barriga, E. Rienks, O. Rader, R. Calarco, G. Bihlmayer *et al.*, Evidence for topological band inversion of the phase change material $GeSb_2Te_5$, Appl. Phys. Lett. **103**, 243109 (2013).

[28] J. Kellner, G. Bihlmayer, V. L. Deringer, M. Liebmann, C. Pauly, A. Giussani, J. E. Boschker, R. Calarco, R. Dronskowski, and M. Morgenstern, Exploring the subsurface atomic structure of the epitaxially grown phase-change material Ge_2Sb_2Te, Phys. Rev. B **96**, 245408 (2017).

[29] M. Neupane, A. Richardella, J. Sanchez-Barriga, S. Xu, N. Alidoust, I. Belopolski, C. Liu, G. Bian, D. Zhang, D. Marchenko *et al.*, Observation of quantum-tunnelling-modulated spin texture in ultrathin topological insulator Bi_2Se_3 films, Nat. Commun. **5**, 3841 (2014).

[30] J. Seo, P. Roushan, H. Beidenkopf, Y. S. Hor, R. J. Cava, and A. Yazdani, Transmission of topological surface states through surface barriers, Nature (London) **466**, 343 (2010).

[31] K. Kuroda, G. Eguchi, K. Shirai, M. Shiraishi, M. Ye, K. Miyamoto, T. Okuda, S. Ueda, M. Arita, H. Namatame *et al.*, Tunable spin current due to bulk insulating property in the topological insulator $Tl_{1\text{-}x}Bi_{1+x}Se_{2-\delta}$, Phys. Rev. B **91**, 205306 (2015).